Proc. NAFEMS World Congress'99 on
Effective Engineering Analysis, Vol. 1, pp. 297-309

DEVELOPMENT AND APPLICATION OF A FINITE VOLUME METHOD FOR STATIC AND TRANSIENT STRESS ANALYSIS

P.J.Oliveira [a] , C.J.Rente [b]

SUMMARY

A wide variety of physical problems in continuum mechanics are commonly treated by numerical methods and, among these, the Finite Element Method (FEM) has found widespread scope for application.

On the other hand, Finite Volume Methods (FVM) were initially developed in connection with computational fluid dynamics applications but can, in principle, be extended for the solution of solid stress analysis problems.

In this paper, a finite volume method is presented for the solution of static and transient problems in the field of structural mechanics. This paper is thus aimed at introducing finite volume techniques, with their possible advantages, in a field traditionally dominated by finite element methods.

A detailed description of the FV method developed will be given in the paper, with emphasis on the treatment of the general discretisation procedure, both in space and in time. The method is valid for curvilinear computational meshes that may be fitted to complex geometries such as those likely to be found in stress analysis. The possibilities of this method will then be assessed from results of application to some test problems, both in static and in dynamic structural situations. Particular attention will be paid to discretisation in time with view to accurately model transient dynamic situations.

1. INTRODUCTION

Numerical simulations in the field of structural mechanics have traditionally been performed with the Finite Element Method (FEM) while Finite Volume Methods (FVM) have enjoyed an undivided popularity as a very efficient way of solving problems in the area of fluid flow. In the past few years some effort has been made to introduce FEM in fluid flow calculations, but the dissemination in the opposite direction has not occurred in similar proportion and the international scientific community seems

[a] Professor Associado, Departamento de Engenharia Electromecânica, Universidade da Beira Interior, Rua Marquês D'Ávila e Bolama, 6200 Covilhã, Portugal
[b] Professor Adjunto, Departamento de Engenharia Civil, Instituto Politécnico de Tomar, Estrada da Serra, 2300 Tomar, Portugal

unaware of the potential of FVM to solve structural problems. As far as we know there have been only a few works trying to invert this state of things and we emphasise that by Demirdzic *et al*. [2-5] which showed promising perspectives as a viable alternative solver in the field of solid stress analysis. The FVM is usually second-order accurate in space, is based on integral forms of the governing equations and uses a segregated solution procedure for solving iteratively a set of algebraic equations associated with diagonally dominant matrices. The main advantage of FVM in fluid flow is related to its efficiency to treat complex mathematical models with both coupled and non-linear differential equations of large matrices. This advantage can be exploited in the treatment of other problems in continuum mechanics and in particular in structural analysis. In this paper we examine the performance of a FV method, originally developed for fluid flow calculations, and here adapted to the treatment of linear elastic-solid behaviour in general three-dimensional domains with complex geometry. Many of the questions arising in the extension of FVM to steady-state stress analysis have received attention in the work of Demirdzic *et al* [2-5] and also in [8]. And so emphasis is here on the treatment of transient problems. FVM procedures often utilise explicit or fully-implicit discretisation schemes to deal with time-dependent problems, namely the Euler-based methods or multipoint methods, like the Cranck-Nicolson scheme. Here, we examine other type of methods that are common in FEM so as their merits can be assessed. Two test cases are considered: stress concentration around circular and elliptic holes, and the transient response of a beam clamped at both ends.

2. GOVERNING EQUATIONS

The equations to be solved are those governing the behaviour of three-dimensional elastic solids. Tensorial notation with implied summation for repeated indices will apply to either Cartesian x_i ($i,j,...$) or curvilinear ξ_l ($l,m,...$) directions, as shown in Fig.1.

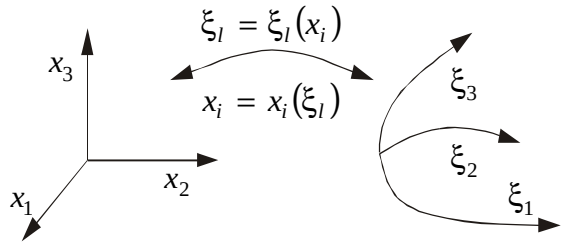

Fig.1. Schematic representation of the transformation of a rectangular Cartesian system to a non-orthogonal co-ordinate system that follows the mesh lines.

The momentum conservation equation, expressing Newton's second law for an arbitrary portion of solid with volume V, is written in differential form, referred to a rectangular Cartesian system, as:

$$\frac{\partial^2(\rho u_i)}{\partial t^2} = \frac{\partial \sigma_{ij}}{\partial x_j} + \rho g_i \tag{1}$$

In (1), ρ is the solid density, u_i are the displacement vector components, σ_{ij} are the stress tensor components and g_i are body force components, typically the gravity acceleration. The constitutive equation for a linear elastic body relates the stress tensor to the displacement vector and follows Hook's law:

$$\sigma_{ij} = \mu\left(\frac{\partial u_i}{\partial x_j} + \frac{\partial u_j}{\partial x_i}\right) + \lambda \frac{\partial u_k}{\partial x_k}\delta_{ij} \tag{2}$$

where δ_{ij} is the Kronecker symbol and μ and λ are Lame's coefficients. These can be expressed in terms of the usual values for Young's modulus E and the Poisson's ratio ν, through the following generic expressions:

$$\mu = \frac{E}{2(1+\nu)} \quad \text{and} \quad \lambda = \frac{\nu E}{(1+\nu)(1-2\nu)} \tag{3}$$

For a plane stress problem, the particular case to be considered in the present work, the equations will retain the same form as the general equations given above, if the Lame coefficient λ is defined in a different way as:

$$\lambda = \frac{\nu E}{(1+\nu)(1-\nu)} \tag{4}$$

After introducing the constitutive Eq. (2) into the momentum balance Eq. (1), this can be rewritten as

$$\frac{\partial^2 u_i}{\partial t^2} - \frac{\partial}{\partial x_j}\left(\mu \frac{\partial u_i}{\partial x_j}\right) = \frac{\partial}{\partial x_i}\left(\mu \frac{\partial u_j}{\partial x_i}\right) + \frac{\partial}{\partial x_i}\left(\lambda \frac{\partial u_k}{\partial x_k}\right) + \rho g_i \tag{5}$$

thus representing a set of three partial differential equations of elliptic type, to be solved for the 3 displacement components aligned with the Cartesian co-ordinates. Once the u_i are known, the components of the stress tensor can then be obtained from Eq. (2) and a generic traction vector T_i related to a surface with a normal unit vector n_i is given by:

$$T_i = \sigma_{ij} n_j = \mu\left(n_j \frac{\partial u_i}{\partial x_j} + \frac{\partial n_j u_j}{\partial x_i}\right) + \lambda \frac{\partial u_k}{\partial x_k} n_i \tag{6}$$

To complete the mathematical model, initial and boundary conditions must be given. As initial conditions, at $t = t_0$, we take given displacement vector over the entire solution domain. Boundary conditions must be specified at all times, due to the elliptic nature of the mathematical model, and can be of the following three types:

- Dirichlet boundary conditions, where prescribed displacements are given at the boundary Γ_D
- Neumann boundary conditions, where prescribed tractions are given at the boundary Γ_N

- Symmetry planes, where the tangencial u_τ and the normal u_n displacement vector components at the boundary Γ_S, defined by the normal direction n, must obey to the relations $u_n = 0$ and $\dfrac{\partial u_\tau}{\partial n} = 0$

The last condition is a mathematical condition resulting from division of the original domain based on symmetry. The purpose is to reduce the size of the solution domain. The total boundary of the solution domain D must equal the sum of the different boundary types: $\partial D = \Gamma_D + \Gamma_N + \Gamma_S$.

3. NUMERICAL METHOD

3.1. Introduction

In the finite volume method the computational domain is divided into contiguous hexahedral cells with arbitrary orientation, and the differential equations are then integrated over each cell. The various terms in the equations are discretised by means of central differences in the mesh formed by all those cells, with the variables stored at the centre of the cells. The end result of the discretisation is a set of algebraic equations relating centre of cell values of the unknown variables to their values at near-by cells. After being linearised, if the need arises, that system is solved by a conjugate-gradient method as explained in [6]. In order to deal with arbitrary geometries there is the need to transform the equations from Cartesian co-ordinates to the general non-orthogonal co-ordinates, and this can be performed easily by applying the transformation rule [7;8]:

$$\frac{\partial}{\partial x_i} = \frac{\partial}{\partial \xi_l}\frac{\partial \xi_l}{\partial x_i} = \frac{1}{J}\frac{\partial}{\partial \xi_l}\beta_{li} \tag{7}$$

where J is the Jacobian of the transformation $x_i = x_i(\xi_l)$ and β_{li} are metric coefficients defined as the cofactor of $\partial x_i / \partial \xi_l$.

The integration of the governing equations written in generalised co-ordinates is straightforward after an acquaintance with the nomenclature introduced in Fig.2.

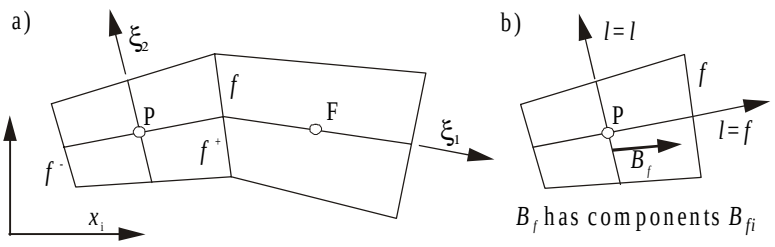

Fig.2. Some nomenclature: a) generic and neighbouring cells; b) area vectors and components

In fact, it suffices to replace: the β_{li} coefficients by the Cartesian i-components of the surface along direction *l*, denoted B_{li}; the Jacobian *J* by the cell volume V; and the derivatives $\partial/\partial\xi_l$ by differences between values along direction *l*.

3.2. Discretisation of the equations

Application of the transformation rule (7) to Eq. (1) leads to the final form of the governing equations:

$$\frac{\partial^2(J\rho u_i)}{\partial t^2} = \frac{\partial}{\partial\xi_l}\left(\beta_{lj}\sigma_{ij}\right) + J\rho g_i \tag{8}$$

Integration over a cell V_P of each term in this equation is now discussed.

- Inertia term

  $$\int_{V_P} \frac{\partial^2}{\partial t^2}(J\rho u_i)\,\mathrm{d}V$$

  can have different forms depending on the time discretisation. To simplify the explanation of the discretisation schemes, we re-write (8) as:

  $$\frac{\partial^2\psi}{\partial t^2} = F(u,t) \qquad \text{where } \psi = \int_{V_P} J\rho u_i\,\mathrm{d}V \tag{9}$$

  The left-hand side can be integrated exactly over a given time step δt, from t_n to $t_{n+1} = t_n + \delta t$, while the right hand side requires an approximation for the mean value of the function $F(u,t)$ prevailing over that time step. The *Implicit-Euler* method utilises the value at the end of the time step $F\left(u^{t+\delta t}, t+\delta t\right)$ but is only first-order in time; to improve accuracy one can use the second-order *Crank-Nicolson* scheme, in which case the approximation for *F* is the average of the old and the new value of the function $\frac{1}{2}\left[F\left(u^{t+\delta t}, t+\delta t\right) + F\left(u^{t}, t\right)\right]$. In both cases, the time-derivative (inertia) term is discretised as:

  $$\int_{V_P} \frac{\partial^2}{\partial t^2}(J\rho u_i)\,\mathrm{d}V = \frac{\rho V_P}{\delta t^2}\left(u_{i,P}^{t+\delta t} - 2u_{i,P}^{t} + u_{i,P}^{t-\delta t}\right) \tag{10}$$

  A different second-order scheme is obtained if the integration involves three time levels over an interval centered around the new time level t_{n+1}, i.e., from $t_{n+1} - \delta t/2$ to $t_{n+1} + \delta t/2$. This is the popular *Three-Time Level* in which the function F of Eq. (9) is evaluated at the new time level as in the Implicit Euler and the inertia term is now given by

  $$\int_{V_P} \frac{\partial^2}{\partial t^2}(J\rho u_i)\,\mathrm{d}V = \frac{\rho V_P}{2\delta t^2}\left(3u_{i,P}^{t+\delta t} - 7u_{i,P}^{t} + 5u_{i,P}^{t-\delta t} - u_{i,P}^{t-2\delta t}\right) \tag{11}$$

The schemes just described are rooted on FVM for computational fluid dynamics. Instead, time integration can follow methods well known to FEM practitioners. We present two of them: the Houbolt method, which has some similarity with the differencing scheme of the FVM approach; and the Newmark method, which is a classic and efficient method to deal with time-dependent structural analysis problems. In both, the function $F(u,t)$ in Eq. (9) is evaluated at the new time level $F\left(u^{t+\delta t}, t+\delta t\right)$. The *Houbolt* integration [1] uses standard difference expressions to approximate the velocity and acceleration components in terms of displacement components based on backward-difference formulae. After some manipulation, the resulting inertia term at t_{n+1} is:

$$\int_{V_P} \frac{\partial^2}{\partial t^2}\left(J\rho u_i\right)\mathrm{d}V = \frac{\rho V_P}{\delta t^2}\left(2u_{i,P}^{t+\delta t} - 5u_{i,P}^{t} + 4u_{i,P}^{t-\delta t} - u_{i,P}^{t-2\delta t}\right) \tag{12}$$

showing a stronger contribution on the implicit term $u(t+\delta t)$, compared with the previous schemes. As in the Three Time Level scheme, however, there is the need to store variable values at the three previous time levels.

The *Newmark* integration scheme [1] is an extension of the linear acceleration method in which the following assumptions are made:

$$\mathrm{v}_{i,P}^{t+\delta t} = \mathrm{v}_{i,P}^{t} + \left[(1-\alpha)\,\mathrm{a}_{i,P}^{t} + \alpha\,\mathrm{a}_{i,P}^{t+\delta t}\right]\delta t \tag{13}$$

$$u_{i,P}^{t+\delta t} = u_{i,P}^{t} + \mathrm{v}_{i,P}^{t}\,\delta t + \left[(0.5-\beta)\,\mathrm{a}_{i,P}^{t} + \beta\,\mathrm{a}_{i,P}^{t+\delta t}\right]\delta t^2 \tag{14}$$

Here $\mathrm{v}_{i,P}$ and $\mathrm{a}_{i,P}$ are the velocity and acceleration components, respectively, and α and β are parameters chosen so that accuracy and stability are ensured. In these work we use the constant average acceleration method with $\alpha = 0.5$ and $\beta = 0.25$ initially proposed by Newmark. Eqs.(13-14) can be manipulated to express the velocity and acceleration at the new time level in terms of the unknown displacements only, and the inertia term is therefore given by

$$\int_{V_P} \frac{\partial^2}{\partial t^2}\left(J\rho u_i\right)\mathrm{d}V = \rho V_P\left(\frac{u_{i,P}^{t+\delta t} - u_{i,p}^{t}}{\beta\delta t^2} - \frac{\mathrm{v}_{i,P}^{t}}{\beta\delta t} - \left(\frac{1}{2\alpha}-1\right)\mathrm{a}_{i,P}^{t}\right) \tag{15}$$

- Stress-divergence term

$$\int_{V_P} \frac{\partial}{\partial \xi_l}\left(\beta_{lj}\sigma_{ij}\right)\mathrm{d}V = \sum_{f}^{6}\left(B_f T_{i,f}\right) \tag{16}$$

where *f* denotes the faces of the general cell P and B_f is the scalar area of the face *f*. Clearly, Eq. (16) represents the balance of the internal forces applied to the surface of the cell. From Eq. (6) each term of Eq. (16) transformed into curvilinear co-ordinates becomes

$$B_f T_{i,f} = \frac{\mu_f}{V_f}\left(B_{fj}B_{lj}\frac{\partial u_i}{\partial \xi_l} + B_{fj}B_{li}\frac{\partial u_j}{\partial \xi_l}\right)_f + \frac{\lambda_f}{V_f}\left(B_{fi}B_{lk}\frac{\partial u_k}{\partial \xi_l}\right)_f \tag{17}$$

where the derivatives $\partial/\partial\xi_l$ will be evaluated as differences between values along direction *l*, for example $\left(\frac{\partial u_i}{\partial \xi_l}\right)_f = [\Delta u_i]_f^l = u_{i,F} - u_{i,P}$ for $l=f$ (Fig.2).

- Gravity or body-force term

$$\int_{V_P} J\rho g_i \, \mathrm{d}V = \rho V_P g_i \tag{18}$$

The final form of the momentum balance is obtained after re-grouping the various terms to give, in a compact form:

$$a_P \, u_{i,P} - \sum_F^6 \left(a_F \, u_{i,F}\right) = S_i \tag{19}$$

which represents a set of three systems of algebraic equations to be solved for the unknown displacements $u_{i,P}$. The terms written on the left-hand side of (19) are treated implicitly and the coefficients a_P and a_F of the matrix are given by

$$a_P = \sum a_F + a_{inertia} \qquad a_F = \left(\mu_f + \lambda_f\right) B_f^2 / V_f \tag{20}$$

where $a_{inertia}$ represents the contribution of the inertia term and depends on the time integration scheme. The source term S_i is treated explicitly and groups all the terms given by Eqs.(10-12) and Eqs.(15-18) not included in the coefficients. The resulting system matrix Eq. (19) is symmetric positive-definite and well-structured (with only seven nonzero diagonals in 3-D) allowing the solution of the equations by some efficient solver which takes into account these features. In this work, we use a symmetric conjugate gradient solver pre-conditioned with incomplete Cholesky decomposition [6]. The boundary conditions are easily incorporated. For a Dirichlet boundary with a prescribed displacement applied to a cell face of a generic control volume, it suffices to add the contribution $a_F u_i^{presc}$ to the source term and a_F to the central coefficient a_P (as in Eq. (20)), and set $a_F = 0$. For a Neumann boundary condition, we have to add the prescribed traction to the source term and make the coefficient $a_F = 0$.

4. TEST CASES

The capabilities, accuracy and geometrical flexibility of the present Finite Volume methodology are demonstrated in this section on two test cases. The first is a steady-state problem aimed to validate its accuracy in the field of stress concentration. The second one is a transient case suitable to compare the accuracy of the time integration schemes described in section 3.

4.1. Stress concentration around elliptic and circular holes on a flat plate

A finite plate with a elliptic hole in its center is loaded by a unidirectional uniform tension, cf. Fig.3 a).

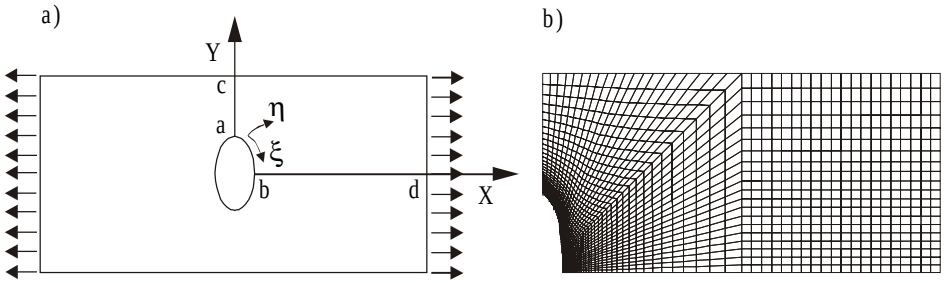

Fig 3. Plate with a central elliptic hole subjected to unidirectional tensile load : (a) geometry and dimensions , (b) numerical grid. (σ_x = 10000 Pa, E = 10^7 Pa, ν = 0.3)

For a very long plate the stress-concentration factor, $k = \sigma_{max}/\sigma_{nom}$, is given as a function of the tensile applied load and the geometric parameters a, b and c by [10]:

$$\sigma_{nom} = \frac{c\,\sigma_x}{(c-a)} \qquad \text{and} \qquad k = k_1 + k_2\left(\frac{a}{c}\right) + k_3\left(\frac{a}{c}\right)^2 + k_4\left(\frac{a}{c}\right)^3$$

where for $0.5 \le a/b \le 10.0$

$$k_1 = 1 + \frac{2a}{b} \qquad k_2 = -0.351 - 0.021\sqrt{(a/b)} - 2.483\,a/b$$

$$k_3 = 3.621 - 5.183\sqrt{(a/b)} + 4.494\,a/b \qquad k_4 = -2.270 + 5.204\sqrt{(a/b)} - 4.011\,a/b$$

By taking into account the symmetry of the problem, the analysis was performed on only one quarter of the solution domain in a mesh with 2000 cells with c = 5 m and b = 0.5 m, as shown in Fig.3 b). In order to reduce the influence of the finite plate dimension in the *x*-direction, a relation d/c = 2 was imposed and mesh spacing was concentrated near the hole by use of suitable mesh expansion factors. We are interested in the value of the maximum stress, occurring at y = a, and the relative error between the numerical predictions and the above solution when the a/b relation varies from 0.5 to 4 is plotted in Fig.4. The accuracy of the results is excellent for a/b relations inferior to unity (major ellipse axis through the *x*-direction). When a/b equals unity the ellipse becomes a circle and for this case the error is also insignificant (0.66%). As we increase the a/b relation, the ellipse became more slender and the error is seen to increase, possibly due to the greater effects of the imposed finite geometry. For the situation corresponding to a = 4b the error in the maximum-stress is 3.15%; for this case we give in Fig.4 the σ_{xx} -stress distribution around the ellipse, clearly revealing the concentration of stresses around the top point in the ellipse.

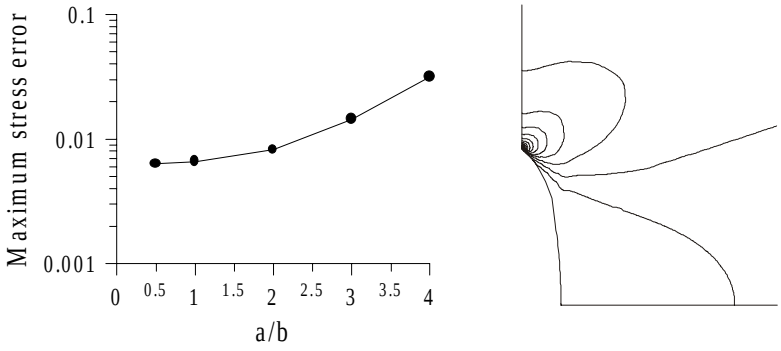

Fig. 4. Maximum stress error for various relations of a/b (left) and stress σ_{xx} distribution around the ellipse (right) for a/b=4 (contour levels from 5000 to 100000, step 5000 Pa).

For the case of a circular hole (a/b = 1) in an infinitely large plate there exists an analytical solution that allows a more precise assessment of the accuracy of our numerical method [2,8]:

$$\sigma_{xx} = \sigma_x \left[1 - \left(\frac{a}{r}\right)^2 \left(\frac{3}{2} cos\, 2\theta + cos\, 4\theta \right) + \frac{3}{2} \left(\frac{a}{r}\right)^4 cos\, 4\theta \right] ,$$

$$\sigma_{yy} = \sigma_x \left[- \left(\frac{a}{r}\right)^2 \left(\frac{1}{2} cos\, 2\theta - cos\, 4\theta \right) - \frac{3}{2} \left(\frac{a}{r}\right)^4 cos\, 4\theta \right] , \qquad (21)$$

$$\sigma_{xy} = \sigma_x \left[- \left(\frac{a}{r}\right)^2 \left(\frac{1}{2} sin 2\theta + sin 4\theta \right) + \frac{3}{2} \left(\frac{a}{r}\right)^4 sin 4\theta \right]$$

where r and θ are the usual polar co-ordinates $r = \sqrt{x^2 + y^2}$ and $\theta = tan^{-1}(y/x)$.

In this test case, the stress distribution given by the solution of Eq. (21) is prescribed at the external boundary of a finite solution domain correspondingly to c = d = 2.0 m; additionally, zero traction is specified at the hole and symmetry conditions at the symmetry axis. This solution domain was discretised with 1600 cells and the numerical results obtained were generally in good agreement with the exact solution. As an example, in Fig. 5 the predicted σ_{xx} stress distribution is compared with the exact solution and the shapes of the stress iso-lines are seen to agree quite well.

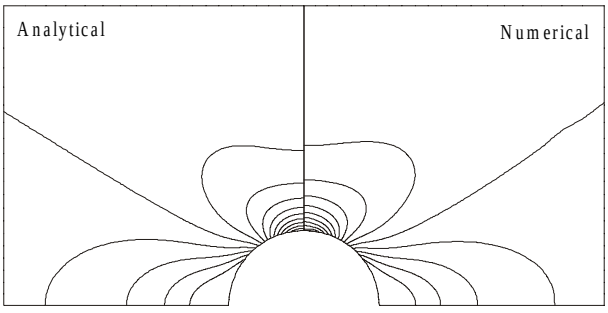

Fig. 5. Stress distribution σ_{xx} (contour levels from 2000 to 30000, step 2000 Pa).

4.2. Transient response of a beam clamped at both ends

In the second example we consider a beam 20 cm long and 1 cm wide, with a Young modulus of 100 GPa, a Poisson ratio of 0.3 and a density of 0.025 kg/cm$^{3.}$ This beam is clamped at both ends and it then subjected to a suddenly applied transversal load of 3 MPa. The analysis is carried out under plane stress and, by symmetry considerations, only half of the beam is considered. In order to investigate the dependence of the numerical results on the grid and time-steps adopted, four meshes (Mesh 1 - 20x2 CVs; Mesh 2 - 40x4 CVs; Mesh 3 - 80x8 CVs and Mesh 4 - 200x20 CVs) and three time steps (10^{-4}s, 10^{-5}s and 10^{-6}s) are considered. The calculations were initially performed on the finest grid and with the smallest time step. For these conditions, the results with the Crank-Nicolson scheme were identical to the solution obtained by modal superposition, where the first five modes of vibration were considered, which we take as representatives of the exact solution.

The central displacement error and the amplitude decay (due to numerical dissipation), for the different time-marching schemes of Section 3, are shown in Fig.6 as a function of $\Delta t/\Delta x$. This figure allows the simultaneous perception of the effects of grid or time-step changes. Each block of curves corresponds, from left to right, to an increasing value of the time-step. For a given block, at constant time-step, increased grid refinement (small Δx) has the effect of reducing the displacement error (Fig. 6 a).

Overall, the results show that fine meshes are crucial to obtain accurate predictions (both in terms of displacement and numerical dissipation) and this particularly true for the smallest time-step. The artificial damping was negligible for all the schemes with the smallest time step and thus it is not represented in Fig.6 b). For the medium time step, 10^{-5}s, the different behaviour of the schemes is accentuated, with reduction in the error with mesh refinement and the Crank-Nicolson scheme giving the best results followed by the Newmark and Houbolt schemes. These give better central displacements results than the Implicit Euler or the Implicit 3 Times Level due to the strongest contribution of the central coefficient, as mentioned in section 3.

In terms of the fictitious amplitude decay, due to numerical dissipation, it clearly increases for the medium time-step, and even more so for the largest time-step. Thus, the time-step has to be kept low for this type of errors to be within reasonable levels. The Newmark and Houbolt schemes are seen to be the best in this respect (cf. Fig 6 b at the medium Δt). The disturbance seen in the displacement error for the largest time step is associated with increased artificial damping due to numerical dissipation when a large Δt is coupled with a small Δx .

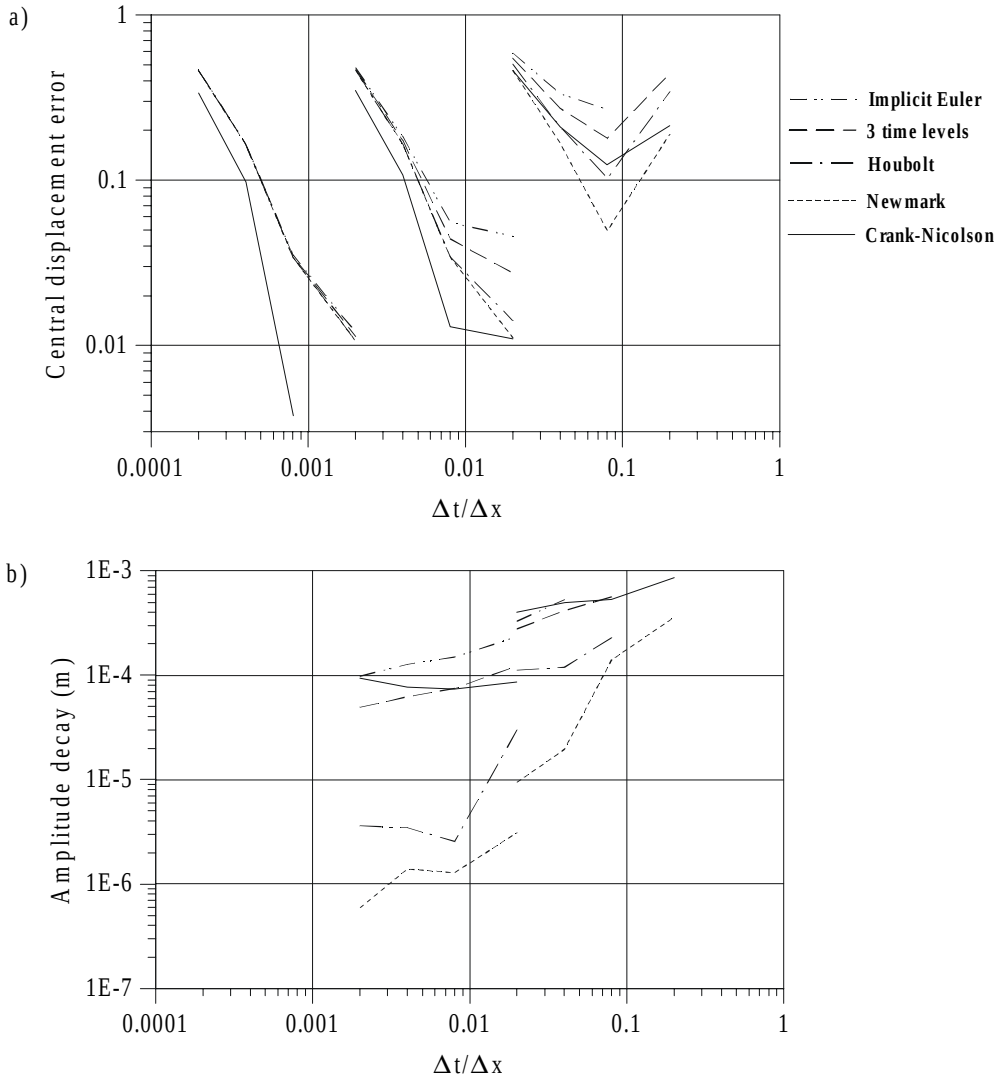

Fig.6. Variation of (a) Central displacement error and (b) amplitude decay with the ratio of the time step to the mesh spacing.

The effect of numerical dissipation in a transient calculation is further illustrated by Fig. 7 a) where the evolution of the central displacement is shown, for the finest mesh and the medium time-step. Even for this fine mesh and relative small time-step, the implicit Euler scheme is seen to introduce too much dissipation and the Newmark again gives the best results.

For an higher value of the time, $\Delta t = 10^{-4}$s, the truncation error becomes non-negligible for all schemes (cf. Fig. 7 b), and even the Newmark then shows some numerical dissipation in time. For the Implicit Euler scheme that dissipation is to such a degree that the expected oscillating results completely dies out after a single oscillation.

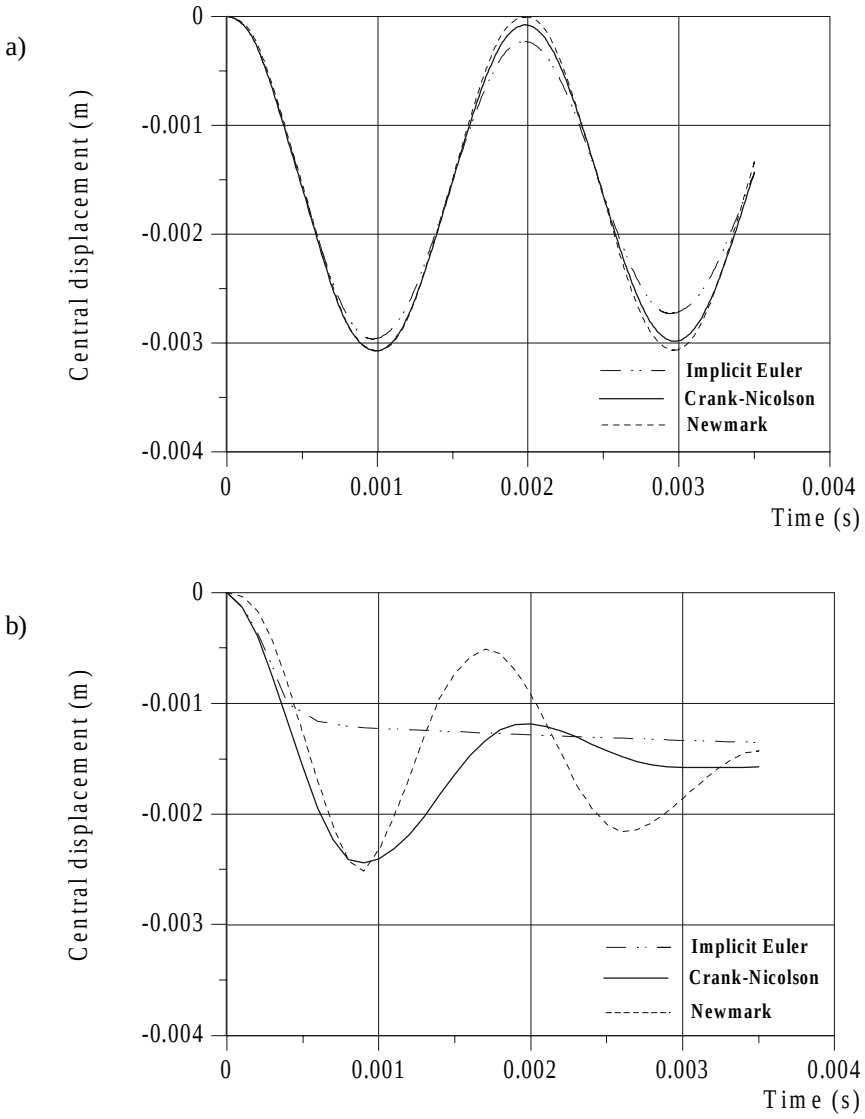

Fig. 7. Central displacement - mesh 4 (200x20CVs) and time steps of (a) 10^{-5}s and (b) 10^{-4}.

5. CONCLUSIONS

The equations for solid elasticity have been discretised and implemented in a finite-volume method. Details of the method are given with focus on the time-differencing scheme used to handle dynamic situations. The method was applied to two test problems, stress concentration around an elliptic hole in a plate and transient response of a beam clamped at both ends. Comparison with available analytical results showed that the method is able to provide predictions with good accuracy. The Crank-Nicolson scheme showed the best behaviour in terms of error reduction with both mesh and time-step refinement; the Newmark scheme is the one which introduces less numerical dissipation.

Compared with standard FEM, the memory requirements are much smaller and thus larger problems may be considered. In terms of solution efficiency, no conclusions could be drawn because no attempt has been made to include required acceleration techniques. This is left for future work.

6. REFERENCES

[1] BATHE, K - Finite Element Procedures in Engineering Analysis, Prentice-Hall, Inc., New Jersey, 1982

[2] DEMIRDZIC, I and MUZAFERIJA, S - Finite Volume Method for Stress Analysis in Complex Domains, Int. J. Numer. Methods Engrg., 37, pp. 3751-3766, 1994

[3] DEMIRDZIC, I and MUZAFERIJA, S - Numerical Method for Coupled Fluid Flow, Heat Transfer and Stress Analysis Using Unstructured Moving Meshes with Cells of Arbitrary Topology, Comput. Meth. Appl. Mech. Engrg., 125, pp. 235-255, 1995

[4] DEMIRDZIC, I, MUZAFERIJA, S and PERIC, M - Bench-Mark Solutions of Some Structural Analysis Problems Using Finite Volume Method and Multigrid Acceleration, Int. J. Numer. Methods Engrg., 40, pp. 1893-1908, 1997

[5] DEMIRDZIC, I, MUZAFERIJA, S and PERIC, M - Advances in Computation of Heat Transfer, Fluid Flow and Solid Body Deformation Using Finite Volume Approaches, Advances in Numerical Heat Transfer, Minkowycz, WJ and Sparrow, EM editors, 1997

[6] MEIJERINK, JA and Van Der Vorst, HA - An iterative solution method for linear systems of which the coefficient matrix is a symmetric M-matrix, Math. of Comp., 31, pp. 148-162, 1977

[7] OLIVEIRA, PJ - Computer Modelling of Multidimensional Multiphase Flow, Ph.D. thesis, Univ. of London, 1992

[8] OLIVEIRA, PJ, REIS, A - Aplicação dum Método de Volumes Finitos ao Cálculo da Concentração de Tensões em Placa Plana com Orifício, V Encontro Nacional de Mecânica Computacional, Universidade do Minho, Portugal, 1997

[9] TIMOSHENKO,SP and GOODIER,JN - Theory of Elasticity, McGraw-Hill Book Company, 1970

[10] YOUNG, WC - Roark's Formulas for Stress & Strain, McGraw-Hill Book Company, 1989